Astron. Astrophys. 187, 502–512 (1987)

ASTRONOMY
AND
ASTROPHYSICS

# Evidence for methane and ammonia in the coma of comet P/Halley

**M. Allen[1,2], M. Delitsky[1], W. Huntress[1], Y. Yung[2], W.-H. Ip[3], R. Schwenn[3], H. Rosenbauer[3], E. Shelley[4], H. Balsiger[5], and J. Geiss[5]**

[1] Jet Propulsion Laboratory, California Institute of Technology, 4800 Oak Grove Drive, Pasadena, CA 91109, USA
[2] Division of Geological and Planetary Sciences, California Institute of Technology, Pasadena, CA 91125, USA
[3] Max Planck Institut fur Aeronomie, D-3411 Katlenburg-Lindau, Federal Republic of Germany
[4] Lockheed Palo Alto Research Laboratory, Palo Alto, CA 94304, USA
[5] Physikalishes Institut, University of Bern, 3012 Bern, Switzerland

Received February 10, accepted April 30, 1987

**Summary.** Methane and ammonia abundances in the coma of Halley are derived from Giotto IMS data using an Eulerian model of chemical and physical processes inside the contact surface to simulate Giotto HIS ion mass spectral data for mass-to-charge ratios ($m/q$) from 15 to 19. The ratio $m/q = 19/18$ as a function of distance from the nucleus is not reproduced by a model for a pure water coma. It is necessary to include the presence of $NH_3$, and uniquely $NH_3$, in coma gases in order to explain the data. A ratio of production rates $Q(NH_3)/Q(H_2O) = 0.01$–$0.02$ results in model values approximating the Giotto data. Methane is identified as the most probable source of the distinct peak at $m/q = 15$. The observations are fit best with $Q(CH_4)/Q(H_2O) = 0.02$. The chemical composition of the comet nucleus implied by these production rate ratios is unlike that of the outer planets. On the other hand, there are also significant differences from observations of gas phase interstellar material.

**Key words:** atomic and molecular processes – comets

## 1. Introduction

The ion mass spectra of the coma of comet Halley are richly complex, as illustrated by the early results published by Balsiger et al. (1986). In this paper we concentrate on the most abundant group of ions in Halley ion mass spectra; the group with masses between 12 and 19 amu. This group of ions contains information on the abundances of water ($H_2O$), methane ($CH_4$), and ammonia ($NH_3$); three of the simplest potential parent molecules containing C, N, and O atoms.

We focus on an analysis of ion processes inside the contact surface (along the Giotto trajectory, ~4600 km from the nucleus; Balsiger et al. 1986) where the ion chemistry is relatively straightforward, and where photoionization is the dominant ionization process. Also, ion flow is predominantly radial in this region, which simplifies the model analysis. This investigation uses the data from the high-intensity spectrometer (HIS) of the Giotto ion mass spectrometer (IMS) experiment. The HIS instrument was optimized specifically for making ion measurements inside the contact surface.

Table 1 shows the ions that potentially could contribute to the peaks in IMS spectra at mass-to-charge ratios ($m/q$) from 12 to 19. In a search for evidence of methane and ammonia in coma gases, we concentrate on the peaks at $m/q = 15$–$19$ in the HIS ion mass spectra (cf. Fig. 8 in Balsiger et al., 1986). The peak at $m/q = 15$ is diagnostic for $CH_3^+$ ions, but with a potential contribution from $NH^+$. Balsiger et al. (1986) have reported that the dominance of the 15 peak relative to 16 over the entire inner coma identifies this peak as mainly $CH_3^+$ rather than $NH^+$. This is because of all ions with $m/q \leq 16$ [i.e., $CH_n^+$ ($n = 0$–$4$), $NH_n^+$ ($n = 0$–$2$), and $O^+$], only $CH_3^+$ does not react with water; the main constituent of the coma. Thus, in a water-dominated coma, the unreactive $CH_3^+$ ions at $m/q = 15$ become prominant at this position in the mass spectrum. This fortunate circumstance allows the identification of the methyl cation in the presence of dominating quantities of water, and allows the identification to be distinguished from $NH^+$ ions. There is no equivalent circumstance in neutral mass spectra. In this paper, we confirm the identification of $m/q = 15$ as $CH_3^+$ and derive a relative production rate of its parent by comparison with chemical modeling of ion-molecule reactions in the coma.

Since water dominates the composition of Halley coma gases, any peaks which might be due to $NH_2^+$ at $m/q = 16$ and $NH_3^+$ at $m/q = 17$ will have significant contributions from $O^+$ and $OH^+$. Contributions from $CH_2^+$ and $CH_3^+$ at $m/q = 14$ and 15

**Table 1.** Ion masses and contributing species

| $m/q$ | Possible species |
|---|---|
| 12 | $C^+$ |
| 13 | $CH^+$ |
| 14 | $CH_2^+$, $N^+$ |
| 15 | $CH_3^+$, $NH^+$ |
| 16 | $CH_4^+$, $NH_2^+$, $O^+$ |
| 17 | $CH_5^+$, $NH_3^+$, $OH^+$ |
| 18 | $NH_4^+$, $H_2O^+$ |
| 19 | $H_3O^+$ |

*Send offprint requests to:* M. Allen

can also mask the identification of $N^+$ and $NH^+$. This makes the identification of small quantities of ammonia exceedingly difficult in both ion and neutral mass spectra of the coma. Ion-molecule chemistry can be used to diagnose the presence of ammonia in this case, but no well-defined peak results as in the case for $CH_3^+$. Instead, the effect of adding ammonia is to significantly alter the ratio of $m/q = 19$ relative to $m/q = 18$. This is because the $H_3O^+$ ion reacts rapidly with $NH_3$ to give $NH_4^+$:

$$H_3O^+ + NH_3 \rightarrow NH_4^+ + H_2O$$

The effect of this reaction is to decrease the 19/18 ratio with increasing ammonia concentration as $H_3O^+$ at $m/q = 19$ is converted to $NH_4^+$ at $m/q = 18$.

We shall show that the 19/18 ion ratio computed for a pure water Halley atmosphere is always too high compared to the HIS data within the contact surface. This suggests that some species is required which preferentially reacts with $H_3O^+$ at $m/q = 19$ relative to $H_2O^+$ at $m/q = 18$. However, any species that reacts with $H_3O^+$ most likely will react with $H_2O^+$ also. This is because the affinity of OH for a proton is less than that of $H_2O$, so that $H_2O^+$ will transfer a proton to a larger suite of chemical species than will $H_3O^+$. Also, $H_2O^+$ has a higher ionization potential than $H_3O^+$ so that it will transfer charge to a larger number of species. $H_2O^+$ is an odd-electron ion and is in general more reactive than $H_3O^+$. Therefore, the effect of adding reactive neutrals to water is to depress the abundances of ions at both $m/q = 18$ and 19, so that the ratio does not change dramatically. The only species so far found to have the desired effect is ammonia, because the product of the reactions of $NH_3$ with both $H_2O^+$ and $H_3O^+$ is $NH_4^+$ at $m/q = 18$. Thus, unless some other species can eventually be found to have this effect, the low 19/18 ion ratio in the coma is best explained by the presence of ammonia. In this way we derive a relative production rate for $NH_3$.

## 2. The coupled transport/chemistry model

The computer model utilized in these calculations is a version of a general one-dimensional coupled transport/chemistry program previously used for studies of the atmospheres of the earth and other planets (e.g., Allen et al., 1981). The model is an Eulerian formulation that solves the continuity equation for each species $i$ self-consistently at a set of fixed distances from the center of the comet nucleus:

$$\frac{\partial n_i}{\partial t} + \frac{1}{r^2}\frac{\partial}{\partial r}(r^2\Phi_i) = P_i + L_i \qquad (1)$$

where $n_i$, $\Phi_i$, $P_i$, and $L_i$ are the concentration, flux, production, and loss rates of $i$ at a distance $r$ and time $t$. These quantities are also functions of $r$. The flux $\Phi_i$ is purely the result of outflowing (or inflowing) material:

$$\Phi_i(r) = n_i(r)v_i(r) \qquad (2)$$

where the velocity $v$ can vary with distance and be different for different species. To seek a numerical solution of (1), with boundary condition (2), we evaluate the spatial variables at a discrete set of points and use time marching for time evolution. The resulting coupled finite difference equations are solved using an implicit method adopted from Richtmeyer (1957). The results of test runs in which a constant outflow velocity and photodestruction scale length were prescribed are found to agree with values derived from the analytical formulation of Haser (1957) to within a few percent. In this paper, the results of steady-state calculations ($\partial n_i/\partial t = 0$) will be presented.

The grid points at which the calculations are performed extend from the surface of the nucleus (assumed to be 7.5 km from the nucleus center) out to a distance of $10^6$ km, with fourteen points per decade of distance. At each grid point, a temperature $T$ and velocity $v$ were prescribed. We adopted a temperature for neutrals, ions, and electrons of 340 K (Balsiger et al., 1986) constant with distance, assuming that the neutral, ion, and electron temperatures are closely coupled inside the contact surface.

Lämmerzahl et al. (1986) report smoothly increasing radial flow speeds from $\sim 1000$ km out to $\sim 30{,}000$ km from the nucleus. Their data inside the contact surface comes from measurements of ion species, while outside the contact surface measurements of neutral species were utilized. Based on their work, we adopted a simple function for the outflow velocity for both ions and neutrals varying with distance: 0.8 km s$^{-1}$ within 1000 km of the nucleus, increasing at a rate of 1.13 cm s$^{-1}$ km$^{-1}$ out to $3\,10^4$ km, and constant at 1.13 km s$^{-1}$ at larger distances. This assumes that a strong coupling between neutral and ion motions exists in the inner coma allowing the neutral species to be assigned the same outflow velocity as the ions.

The lower boundary (nucleus surface) conditions are prescribed for each species in the calculation in the form of a concentration or flux consistent with a desired surface-integrated production rate $Q(i)$. For other than the "parent" species released from the nucleus, the lower boundary condition was zero flux. The upper boundary condition for all species is an outflow velocity of 1.13 km s$^{-1}$.

The solar flux used in the photolysis calculations comes from results of satellite and/or rocket measurements at solar minimum reported by Torr and Torr (1985) for $\lambda \leq 1035$ Å and Mount and Rottman (1983) for $\lambda \geq 1190$ Å. At Lyman alpha, $\lambda = 1215.7$ Å, the solar flux at 1 AU distance from the sun was set to a value of $2.22\,10^{11}$ photons cm$^{-2}$ s$^{-1}$ (R. Clancy, private communication, 1986) as observed by the Solar Mesosphere Explorer satellite (SME; Rottman et al., 1982) on the day of the Giotto encounter with Halley. The solar flux is scaled to the distance of the Giotto encounter. Opacity due to absorption by $H_2O$ in the coma is included in the internal radiation field computation and is allowed to vary as the distribution of $H_2O$ changes. This is a minor effect as the radiation field is attenuated by more than 10% only within a few hundred kilometers of the nucleus surface. In general, it is a good assumption that the photolytic rate constants are constant throughout the coma. Opacity due to the presence of dust in the coma has not been taken into account; we await further reports from the *in situ* and remote observations of Halley.

The discussion in this paper is focussed upon the abundances of light ions – $H_nO^+$, $NH_n^+$, and $CH_n^+$ – within the contact surface. For the purposes of this paper, we calculate the radial distributions of only the "parent" species $H_2O$, $NH_3$, $CH_4$, the neutral "child" species H, O, OH, and the ions $H^+$, $H_{n=0-3}O^+$, $NH_{n=1-4}^+$, and $CH_{n=2-5}^+$. The interrelated chemistry of other species was considered and found not to be important in this spatial region. The key reactions involving these species within the contact surface are listed in Table 2. Total charge neutrality is assumed to hold at all distances; the electron profile is calculated iteratively by summing over the computed positive ion abundances. This is an accurate procedure because the ions with

**Table 2.** Key reactions

| Reaction | Rate constant[a] | Reference |
|---|---|---|
| 1. $H_2O + h\nu \rightarrow$ all products | $1.12\,10^{-5}$[b] $\lambda \leq 1975$ Å | (1) |
| 2. $H_2O + h\nu \rightarrow H + OH$ | $9.37\,10^{-6}$ 610 Å $\leq \lambda \leq 1975$ Å | (1) |
| 3. $H_2O + h\nu \rightarrow 2H + O$ | $6.49\,10^{-7}$ 810 Å $\leq \lambda \leq 1275$ Å | (1) |
| 4. $H_2O + h\nu \rightarrow H_2O^+ + e^-$ | $4.35\,10^{-7}$ $\lambda \leq 983$ Å | (1) |
| 5. $H_2O + h\nu \rightarrow H + OH^+ + e^-$ | $8.32\,10^{-8}$ $\lambda \leq 687$ Å | (1) |
| 6. $H_2O + h\nu \rightarrow H^+ + OH + e^-$ | $3.58\,10^{-8}$ $\lambda \leq 663$ Å | (1) |
| 7. $H_2O + h\nu \rightarrow O^+ +$ products $+ e^-$ | $4.01\,10^{-9}$ $\lambda \leq 662$ Å | (1) |
| 8. $NH_3 + h\nu \rightarrow$ all products | $1.49\,10^{-4}$ $\lambda \leq 2225$ Å | (1) |
| 9. $NH_3 + h\nu \rightarrow NH_3^+ + e^-$ | $8.52\,10^{-7}$ $\lambda \leq 1231$ Å | (1) |
| 10. $NH_3 + h\nu \rightarrow NH_2^+ + H + e^-$ | $2.00\,10^{-7}$ $\lambda \leq 786$ Å | (1) |
| 11. $NH_3 + h\nu \rightarrow NH^+ +$ products $+ e^-$ | $6.07\,10^{-9}$ $\lambda \leq 775$ Å | (1) |
| 12. $NH_3 + h\nu \rightarrow H^+ + 2H +$ products $+ e^-$ | $4.76\,10^{-9}$ $\lambda \leq 681$ Å | (1) |
| 13. $CH_4 + h\nu \rightarrow$ all products | $9.16\,10^{-6}$ $\lambda \leq 1625$ Å | (1) |
| 14. $CH_4 + h\nu \rightarrow CH_4^+ + e^-$ | $4.65\,10^{-7}$ $\lambda \leq 945$ Å | (1) |
| 15. $CH_4 + h\nu \rightarrow CH_3^+ + H + e^-$ | $2.52\,10^{-7}$ $\lambda \leq 866$ Å | (1) |
| 16. $CH_4 + h\nu \rightarrow CH_2^+ +$ products $+ e^-$ | $2.63\,10^{-8}$ $\lambda \leq 822$ Å | (1) |
| 17. $H + h\nu \rightarrow H^+ + e^-$ | $8.09\,10^{-8}$ $\lambda \leq 910$ Å | (1) |
| 18. $O + h\nu \rightarrow O^+ + e^-$ | $2.55\,10^{-7}$ $\lambda \leq 910$ Å | (1) |
| 19. $OH + h\nu \rightarrow O + H$ | $1.50\,10^{-5}$ $\lambda \leq 1925$ Å | (1) |
| 20. $H_2O^+ + e^- \rightarrow H + OH$ | $9.1\,10^{-6}\,T_e^{-0.5}$ | (2) |
| 21. $H_2O^+ + e^- \rightarrow O +$ products | $3.9\,10^{-6}\,T_e^{-0.5}$ | (2) |
| 22. $H_3O^+ + e^- \rightarrow H_2O^+ + H$<br>23. $H_3O + e^- \rightarrow OH + 2H$<br>24. $H_3O^+ + e^- \rightarrow OH +$ other products | $3.39\,10^{-4}\,T_e^{-0.9}$ | (3) |
| 25. $NH_3^+ + e^- \rightarrow H +$ products | $4.1\,10^{-5}\,T_e^{-0.5}$ | estimate |
| 26. $NH_4^+ + e^- \rightarrow NH_3 + H$<br>27. $NH_4^+ + e^- \rightarrow 2H +$ products | $4.1\,10^{-5}\,T_e^{-0.6}$ | (4) |
| 28. $CH_2^+ + e^- \rightarrow$ products | $8.7\,10^{-6}\,T_e^{-0.5}$ | (5) |
| 29. $CH_3^+ + e^- \rightarrow$ products | $1.2\,10^{-5}\,T_e^{-0.5}$ | (5) |
| 30. $CH_4^+ + e^- \rightarrow H +$ products<br>31. $CH_4^+ + e^- \rightarrow 2H +$ other products | $1.2\,10^{-5}\,T_e^{-0.5}$ | (5) |
| 32. $H^+ + H_2O \rightarrow H_2O^+ + H$ | $8.2\,10^{-9}$ | (6) |

[a] Photolytic rate constants are in units of $s^{-1}$, two body rate constants in units of $cm^3\,s^{-1}$.

[b] Values for 0.9 AU with no opacity. Indicated also is the wavelength range in which the cross-sections are significant.

*References:* (1) Allen et al. (1987, in preparation); (2) McGowan et al. (1979); (3) Heppner et al. (1976); (4) Alge et al. (1983); (5) McGowan and Mitchell (1984); (6) Anicich and Huntress (1986).

**Table 2** (continued)

| Reaction | Rate constant[a] | Reference |
|---|---|---|
| 33. $H^+ + CH_4 \rightarrow CH_4^+ + H$ | $1.6\,10^{-9}$ | (6) |
| 34. $H^+ + CH_4 \rightarrow CH_3^+ +$ products | $2.4\,10^{-9}$ | (6) |
| 35. $O^+ + H_2O \rightarrow H_2O^+ + O$ | $3.2\,10^{-9}$ | (6) |
| 36. $OH^+ + H_2O \rightarrow H_2O^+ + OH$ | $1.5\,10^{-9}$ | (6) |
| 37. $OH^+ + H_2O \rightarrow H_3O^+ + O$ | $1.4\,10^{-9}$ | (6) |
| 38. $OH^+ + O \rightarrow H +$ products | $1.0\,10^{-9}$ | Estimate |
| 39. $OH^+ + NH_3 \rightarrow NH_4^+ + O$ | $1.2\,10^{-9}$ | (6) |
| 40. $OH^+ + NH_3 \rightarrow NH_3^+ + OH$ | $1.2\,10^{-9}$ | (6) |
| 41. $H_2O^+ + H_2O \rightarrow H_3O^+ + OH$ | $2.0\,10^{-9}$ | (6) |
| 42. $H_2O^+ + NH_3 \rightarrow NH_3^+ + H_2O$ | $2.2\,10^{-9}$ | (6) |
| 43. $H_2O^+ + NH_3 \rightarrow NH_4^+ + OH$ | $1.0\,10^{-9}$ | (6) |
| 44. $H_3O^+ + NH_3 \rightarrow NH_4^+ + H_2O$ | $2.2\,10^{-9}$ | (6) |
| 45. $NH^+ + H_2O \rightarrow H_3O^+ +$ products | $1.1\,10^{-9}$ | (6) |
| 46. $NH^+ + H_2O \rightarrow H_2O^+ +$ products | $1.1\,10^{-9}$ | (6) |
| 47. $NH^+ + H_2O \rightarrow NH_2^+ + OH$ | $8.75\,10^{-10}$ | (6) |
| 48. $NH^+ + H_2O \rightarrow NH_3^+ + O$ | $1.75\,10^{-10}$ | (6) |
| 49. $NH^+ + H_2O \rightarrow$ other products | $3.5\,10^{-10}$ | (6) |
| 50. $NH_2^+ + H_2O \rightarrow H_3O^+ +$ products | $2.75\,10^{-9}$ | (6) |
| 51. $NH_2^+ + H_2O \rightarrow NH_4^+ + O$ | $1.45\,10^{-10}$ | (6) |
| 52. $NH_3^+ + OH \rightarrow NH_4^+ + O$ | $1.0\,10^{-9}$ | Estimate |
| 53. $NH_3^+ + O \rightarrow$ products | $1.0\,10^{-9}$ | Estimate |
| 54. $NH_3^+ + NH_3 \rightarrow NH_4^+ +$ products | $2.2\,10^{-9}$ | (6) |
| 55. $NH_3^+ + CH_4 \rightarrow NH_4^+ +$ products | $4.8\,10^{-10}$ | (6) |
| 56. $CH_2^+ + H_2O \rightarrow H +$ products | $1.2\,10^{-9}$ | (6) |
| 57. $CH_2^+ + OH \rightarrow H +$ products | $1.0\,10^{-9}$ | Estimate |
| 58. $CH_2^+ + NH_3 \rightarrow H +$ products | $2.5\,10^{-9}$ | (6) |
| 59. $CH_2^+ + CH_4 \rightarrow$ products | $1.2\,10^{-9}$ | (6) |
| 60. $CH_3^+ + OH \rightarrow$ products | $1.0\,10^{-9}$ | Estimate |
| 61. $CH_3^+ + O \rightarrow$ products | $4.4\,10^{-10}$ | (6) |
| 62. $CH_3^+ + NH_3 \rightarrow NH_4^+ +$ products | $3.0\,10^{-10}$ | (6) |
| 63. $CH_3^+ + NH_3 \rightarrow$ other products | $1.29\,10^{-9}$ | (6) |
| 64. $CH_3^+ + CH_4 \rightarrow$ products | $1.2\,10^{-9}$ | (6) |
| 65. $CH_4^+ + H_2O \rightarrow H_3O^+ +$ products | $2.5\,10^{-9}$ | (6) |
| 66. $CH_4^+ + OH \rightarrow$ products | $1.0\,10^{-9}$ | Estimate |
| 67. $CH_4^+ + NH_3 \rightarrow NH_3^+ + CH_4$ | $1.6\,10^{-9}$ | (6) |
| 68. $CH_4^+ + NH_3 \rightarrow NH_4^+ +$ products | $1.5\,10^{-9}$ | (6) |
| 69. $CH_4^+ + NH_3 \rightarrow CH_5^+ +$ products | $6.32\,10^{-11}$ | (6) |
| 70. $CH_5^+ + H_2O \rightarrow H_3O^+ + CH_4$ | $3.7\,10^{-9}$ | (6) |

$m/q \leq 19$ account for almost all of the observed ionization in the inner coma (Balsiger et al., 1986).

### 3. The radial distribution of parent species

The radial profiles of coma ions are directly related to the distribution within the coma of the neutral molecules (usually "parent" species directly released from the nucleus) from which the ions are derived. Few observations of the spatial profiles of parent species have been published for comet Halley with which our model for the neutral precursor species can be verified. However, the distribution of $H_2O$ within $\sim$ 40,000 km of the nucleus is available from the Giotto NMS experiment (Krankowsky et al., 1986).

In a note added in proof, Krankowsky et al. indicate that their published data includes an error in the distance scale, 230 km farther from the nucleus than in actuality. Therefore, we chose to refit the published NMS experimental results, correcting the distances, using the Haser (1957) formulation. Averaging results from each NMS analyzer, we find a value for $Q(H_2O)/v = 4.9\,10^{14}\,cm^{-3}\,km^2$ and, assuming $v = 0.9\,km\,s^{-1}$, $Q(H_2O) = 4.4\,10^{29}\,molec\,s^{-1}$. If $v$ is closer to $0.8\,km\,s^{-1}$, then $Q(H_2O)$ is proportionately smaller. This $Q(H_2O)$ is $\sim$ 20% lower than that reported by Krankowsky et al. and is what is used to derive the model boundary condition for $H_2O$ at the nucleus. A comparable analysis for the NMS $CO_2$ data yields $Q(CO_2)/Q(H_2O) = 0.042$, which is to be compared with the value of 0.035 reported by Krankowsky et al.

The radial profile for $H_2O$ calculated by the model is compared with our representation of the Giotto NMS results in Fig. 1a. Only a small difference between these two curves is noticeable. A more detailed comparison between model results and measurements is shown in Fig. 1b where both $H_2O$ profiles are

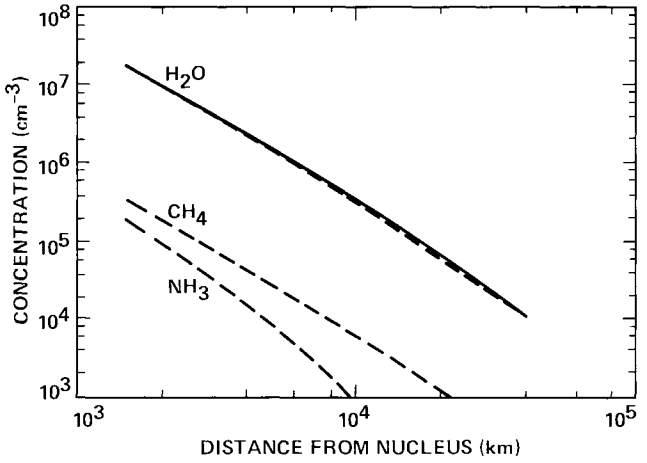


**Fig. 1a.** Comparison of model calculations (dashed lines) of the radial distribution of $H_2O$, $NH_3$, and $CH_4$ with the Giotto neutral mass spectrometer data for $H_2O$ (solid line: Krankowsky et al., 1986).

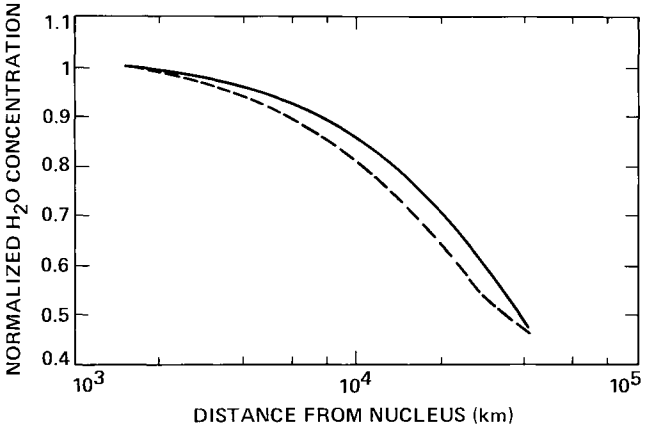


**Fig. 1b.** Giotto NMS results (solid line) and model values (dashed line) for $H_2O$ normalized by the value at the smallest distance and scaled by $r^2$ to correct for spatial dilution from spherical outflow

replotted, scaled by $r^2$, and normalized by the value at the smallest distance. The differences are now more visible, but still the largest discrepancy is only $\sim 7\%$. This manner of presenting the spatial distribution of a species is of interest because the effect of transport and chemistry can be separated. If $H_2O$ were inert, a distribution varying as $r^{-2}$ would be the expected result of the spatial dilution resulting from the radial outflow. This would appear in Fig. 1b as a constant profile with the value of unity. The observed departure from unity reflects the effect of chemical loss.

Krankowsky et al. calculate from their data a value for $v/J(H_2O)$ of $3.9\,10^4$ km, where $J$ is the total photodestruction rate constant for $H_2O$. With $v = 0.9\,\mathrm{km\,s^{-1}}$, $J(H_2O) = 2.3\,10^{-5}\,s^{-1}$. This deduced value for $J(H_2O)$ is much larger than that usually calculated by photochemical models ($\sim 1.1\,10^{-5}\,s^{-1}$) as noted by Krankowsky et al. However, the $J(H_2O)$ derived from a Haser model analysis of the NMS data is reduced significantly after correcting the NMS distance scale and adopting the new estimate of radial velocity. However such an analysis assumes a constant outflow velocity, which is shown to be invalid by the more recent Lämmerzahl et al. (1986) work. Figure 1b shows that the model chemistry summarized in Table 2 reproduces the observed $H_2O$ profile.

As the agreement between observations and model results for one parent species, $H_2O$, is excellent, we feel that other parent species distributions calculated by our model are fairly accurate and have reasonable confidence in our model ion source terms. For later reference we also plot in Fig. 1a the calculated profiles for $NH_3$ and $CH_4$, using values for $Q(NH_3)/Q(H_2O)$ and $Q(CH_4)/Q(H_2O)$ derived below.

## 4. The ratio m/q = 19/18 and the inferred ratio $Q(NH_3)/Q(H_2O)$

Within the contact surface, $H_nO^+$ ions are formed directly from $H_2O$ by ionization and indirectly by charge exchange or by dissociation followed by ionization. These ions react subsequently with $H_2O$ in one or more steps leading to production of $H_3O^+$. This is illustrated in Fig. 2. In a pure $H_2O$ coma, the only loss process for $H_3O^+$ is relatively slow recombination with electrons. As a consequence, $H_3O^+$ at $m/q = 19$ is expected to be the most abundant ion. Figure 3 shows the spatial variation of the ratio $m/q = 19/18$ from HIS spectra compared with the results of model calculations for the pure $H_2O$ coma case. The model shows a different variation with distance than is seen in the HIS data, and the model ratios are significantly higher at the smaller distances.

Unlike the case for methane, it is not possible to identify a specific ion in the HIS spectra as derived from ammonia. The presence of ammonia is inferred from the behavior of the ratio $m/q = 19/18$ with distance from the comet. The important reactions inside the contact surface involving $NH_n^+$ ions are illustrated in Fig. 4. The direct products of $NH_3$ ionization react rapidly with $H_2O$ to form $NH_4^+$ at $m/q = 18$. The proton exchange between $H_3O^+$ and $NH_3$ is a significant loss process for $H_3O^+$ and a major source for $NH_4^+$. The presence of ammonia introduces a mechanism for transferring ion density from mass 19 to mass 18 with a consequent reduction in the ratio $m/q = 19/18$. The results of model runs with varying amounts of ammonia are shown in Fig. 3. It is clear that ammonia is necessary in order to account for the very low 19/18 ratios observed at distances closest to the comet. Values of $Q(NH_3)/Q(H_2O) = 0.01$–$0.02$ result in the best fit to the Giotto data.

Among other likely agents for extracting a proton from $H_3O^+$ is HCN, which has been detected in Halley's coma by its millimeter line emission (Despois et al., 1986; Schloerb et al., 1986; Winnberg et al., 1987). However, the $Q(HCN)/Q(H_2O)$ is only $\sim 10^{-3}$, which is too small to have an appreciable effect on $H_3O^+$. Moreover, if proton transfer to some species other than $NH_3$ were to dominate the loss of $H_3O^+$, then a peak at higher mass comparable to the intensity at $m/q = 19$ would be expected. This is not observed.

Another possible process to reduce the 19/18 ratio is photodissociation of $H_3O^+$. To be important, a photodissociation rate constant of $10^{-3} - 10^{-2}\,s^{-1}$ is necessary. Laboratory cross-sections for this process are unavailable, but a value this large is unlikely. This is illustrated in Table 2 by comparison with the isoelectronic species $NH_3$, whose photodissociation rate constant is much smaller than the required values.

Recently, Murad and Bochsler (1987) proposed a source for $H_3O^+$ not included in our model chemistry: photoionization of the water dimer directly vaporizing from the nucleus and/or sputtered from icy coma grains. If their chemistry were to be included

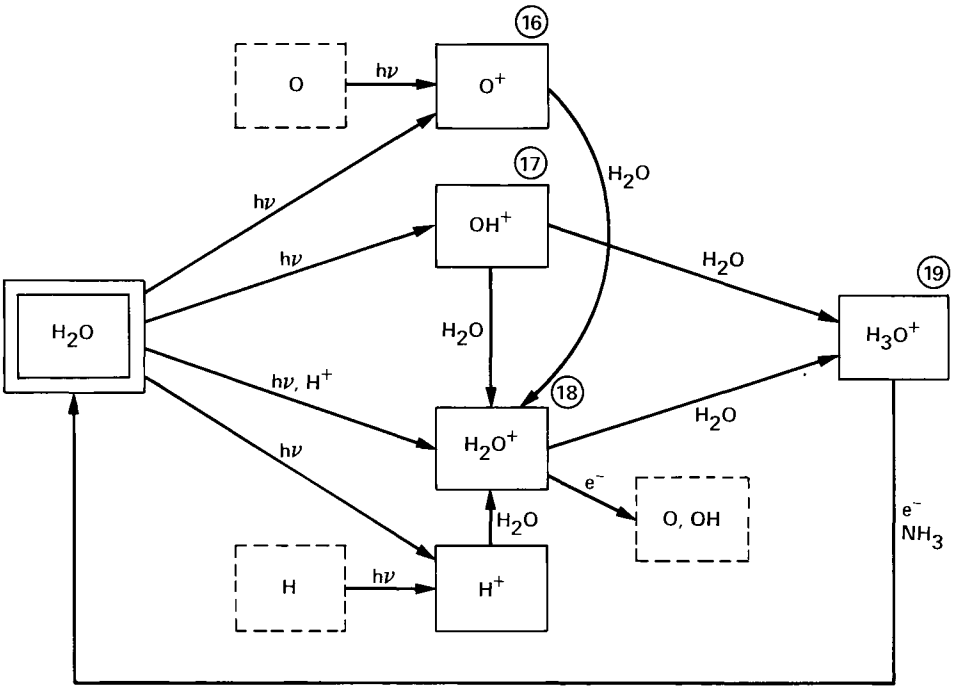


**Fig. 2.** Important reactions for $H_nO^+$ inside of the contact surface. Masses of ions indicated in circles

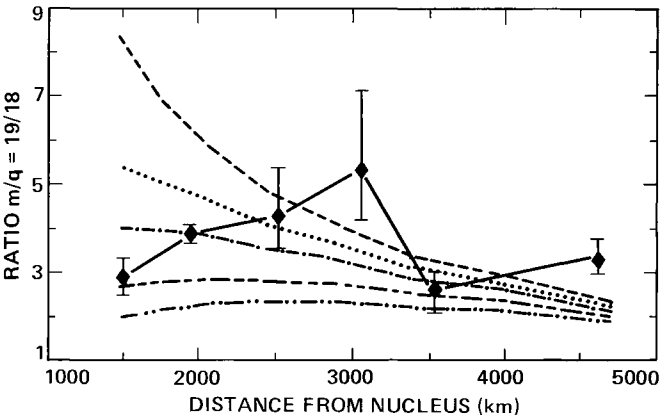


**Fig. 3.** The ratio $m/q = 19/18$ from Giotto HIS measurements (diamonds) compared with model calculations (pure $H_2O$ coma: dashed line; $Q(NH_3)/Q(H_2O) = 0.005$: dotted line; $Q(NH_3)/Q(H_2O) = 0.01$: dash-dot line; $Q(NH_3)/Q(H_2O) = 0.02$: long dash-short dash line; $Q(NH_3)/Q(H_2O) = 0.03$: dash-double dot line). Uncertainties in our estimation of the HIS ratio values are indicated. Giotto values connected by solid lines for visualization purposes

in our model calculations, the model values for the 19/18 ratio would increase, requiring the presence of even more ammonia to fit the Giotto results. Without the availability of absolute ion concentrations, there appears to be no need to add this speculative source of $H_3O^+$ at this time.

The major feature in the data that leads to the necessity to include ammonia is the relatively constant value for the 19/18 ratio with cometary distance, while the prediction for the case without ammonia is significantly different. There are large excursions in the data which are not predicted by the model. We have chosen to weight heaviest in our model/observation comparison the points closest to the nucleus and closest to the contact surface. The reality of the large "bulge" in the 19/18 data will be tested in future analysis of the HIS data. Moreover, reducing the amount of ammonia to fit the central points in Fig. 3 results in a poorer fit at the other $m/q$ ratios to be discussed below.

## 5. The ratio m/q = 15/18 and the inferred ratio $Q(CH_4)/Q(H_2O)$

There are a number of potential sources for the $CH_3^+$ ion identified in the HIS ion mass spectrum. These include the dissociative ionization of methane, hydrocarbons, and other organic compounds containing the methyl ($CH_3$) group: such as methyl acetylene ($CH_3CCH$), methanol ($CH_3OH$), methyl amine ($CH_3NH_2$), and methyl cyanide ($CH_3CN$). Methane is the simplest possible and most efficient per-molecule source of $CH_3^+$, and is a likely candidate for cometary volatiles since it is common in the atmospheres of the outer planets and is the principal carbon-containing molecule in equilibrium solar nebula models. There is also additional evidence in the high-energy-range spectrometer (HERS) ion spectra that support methane as the major source of $CH_3^+$. Balsiger et al. (1986) have reported that the relative abundances of $m/q = 13$–$15$ in HERS data at large distance follow well the predicted behavior for these ions if they were due entirely to methane photolysis and subsequent photoionization.

The important reactions for $CH_n^+$ ions in the inner coma are illustrated in Fig. 5. All of the ions directly produced by photoionization of $CH_4$ react with $H_2O$ except for $CH_3^+$. The dominant loss processes for $CH_3^+$ are electron recombination and reaction with $NH_3$. Because of the latter process, it is necessary

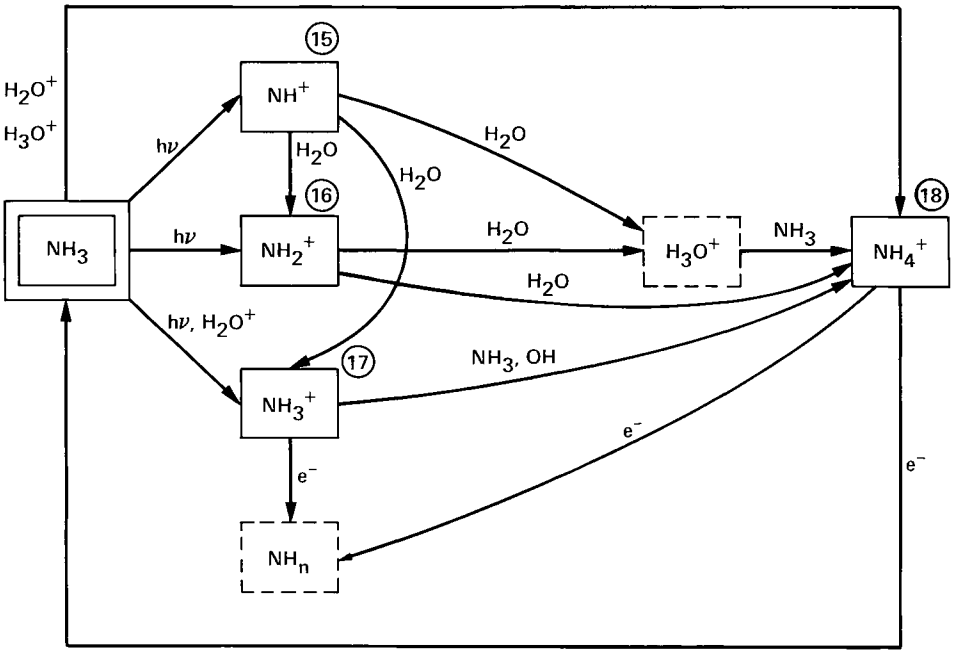


**Fig. 4.** Important reactions for $NH_n^+$ inside of the contact surface. Masses of ions indicated in circles

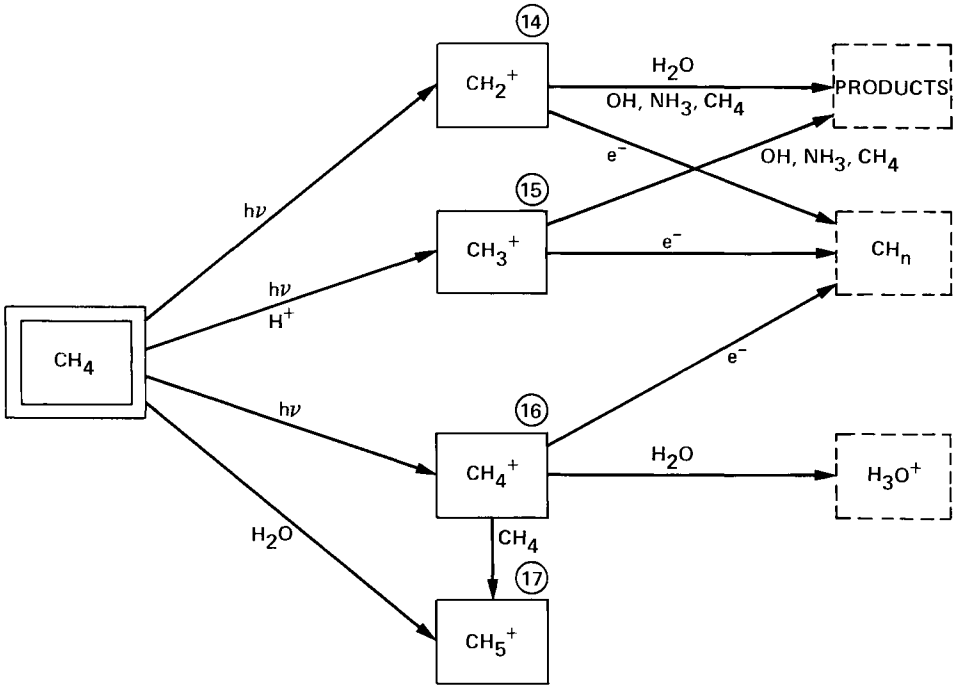


**Fig. 5.** Important reactions for $CH_n^+$ inside of the contact surface. Masses of ions indicated in circles

to determine the ratio $Q(NH_3)/Q(H_2O)$ before modelling the $CH_n^+$ ion chemistry. Figure 6 shows the intensities at $m/q = 15$ relative to 18 in HIS ion spectra inside the contact surface. Shown on the same figure are the results of model runs in which the values for both $Q(CH_4)/Q(H_2O)$ and $Q(NH_3)/Q(H_2O)$ are varied. A comparison of the profiles with and without ammonia shows that $NH_3$ is necessary in the model in order to produce the correct functional form for the abundance of $CH_3^+$ with distance. While the abundance of $NH_3$ is the controlling factor in the shape of the curve, the abundance of $CH_4$ is the controlling factor in the amplitude of the curve. A model with $Q(CH_4)/Q(H_2O) = 0.02$ and $Q(NH_3)/Q(H_2O) = 0.015$ fits the HIS data in Fig. 6 fairly well. Larger amounts of $CH_4$ require larger amounts of $NH_3$ for a reasonable fit, but the $NH_3$ value is already constrained by the 19/18 data. Smaller amounts of $CH_4$ do not produce sufficient $m/q = 15$ at the larger distances.

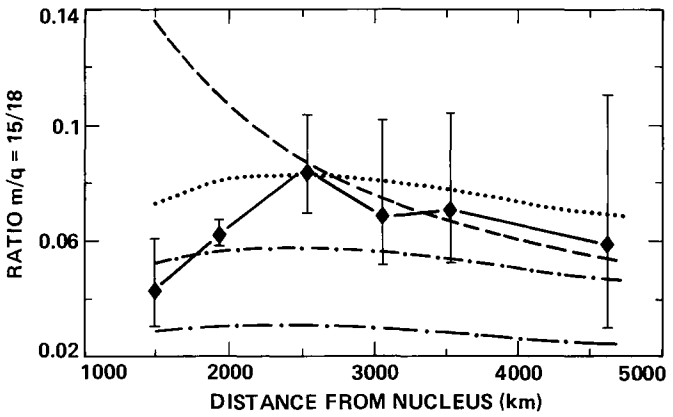


**Fig. 6.** The ratio $m/q = 15/18$ from Giotto HIS measurements (diamonds) compared with model calculations ($Q(CH_4)/Q(H_2O) = 0.02$, $Q(NH_3)/Q(H_2O) = 0$: dashed line; $Q(CH_4)/Q(H_2O) = 0.03$, $Q(NH_3)/Q(H_2O) = 0.015$: dotted line; $Q(CH_4)/Q(H_2O) = 0.02$, $Q(NH_3)/Q(H_2O) = 0.015$: dash-dot line; $Q(CH_4)/Q(H_2O) = 0.01$, $Q(NH_3)/Q(H_2O) = 0.015$: long dash-short dash line). Uncertainties in our estimation of the HIS ratio values are indicated. Giotto values connected by solid lines for visualization purposes

## 6. Further tests of the derived relative production rates for $NH_3$ and $CH_4$

The remaining major distinguishable peak in the mass range $m/q = 13$–$19$ spectra inside the contact surface is $m/q = 17$. The $m/q = 16$ ion appears as a shoulder between $m/q = 15$ and 17 in HIS ion spectra and is contaminated by overlap counts from 15 and 17. Figure 7 shows the 17/18 ratio versus cometary distance compared to a pure $H_2O$ model ($CH_5^+$ abundances are insignificant) and a model with $Q(NH_3)/Q(H_2O)$ and $Q(CH_4)/Q(H_2O)$ as inferred above. The model with ammonia fits the data much better than that without ammonia. Ammonia adds $NH_3^+$ ions to the existing $OH^+$ ions to make up needed ion density at $m/q = 17$. It is significant that ammonia appears necessary to fit the ion density versus distance at every mass where ammonia would have the appropriate effect.

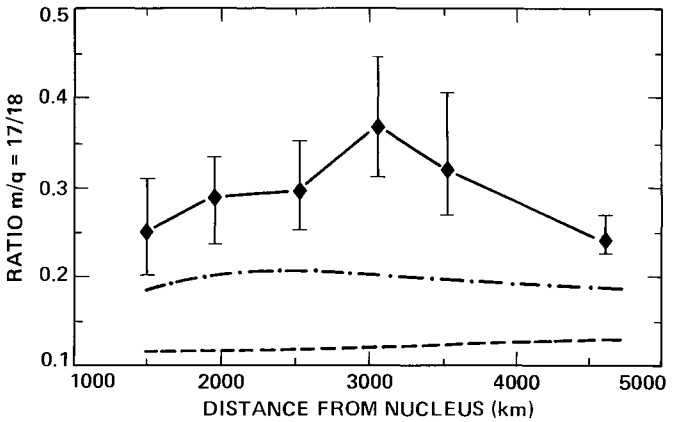


**Fig. 7.** The ratio $m/q = 17/18$ from Giotto HIS measurements (diamonds) compared with model calculations (pure $H_2O$ coma: dashed line; $Q(CH_4)/Q(H_2O) = 0.02$, $Q(NH_3)/Q(H_2O) = 0.015$: dash-dot line). Uncertainties in our estimation of the HIS ratio values are indicated. Giotto values connected by solid lines for visualization purposes

One further test was applied to examine the consistency between HIS and HERS data regarding the presence of ammonia. HERS spectra were taken primarily at large distances beyond the photodissociation scale length for ammonia. The ultimate photodissociation product from $NH_3$ is the N atom. We examined HERS ion mass spectra at ranges from 100,000–200,000 km from the nucleus to determine an upper limit for the amount of $N^+$ ($m/q = 14$) relative to $O^+$ ($m/q = 16$) and hence an upper limit for the amount of N from $NH_3$ photolysis relative to O from $H_2O$ photolysis. At these ranges, water is largely dissociated, but carbon monoxide is not, so that almost all $O^+$ ions in the ion mass spectrum originate from photolysis of $H_2O$ to O atoms via several steps, followed by ionization. For the purpose of this exercise we assumed photoionization to be the major source of ionization with rates of $3\,10^{-7}\,s^{-1}$ for O and $2\,10^{-7}\,s^{-1}$ for N. All $m/q = 14$ ions are assumed to be $N^+$ from $NH_3$ photoprocessing, and the loss rate for all ions is assumed equal via transport. The result is a maximum $NH_3/H_2O$ ratio of 2%. Considering the assumptions involved and the errors in measurement, this is consistent with the ratio determined from HIS ion spectra in the inner coma.

Carbon, nitrogen, and oxygen in the form of both ions and radical compounds have been detected by other experiments on Halley spacecraft and from terrestrial platforms. A detailed comparison with these data awaits further information about the observing geometries. While the evidence for the presence of ammonia and methane seems fairly conclusive from HIS ion mass spectra, the value derived for the relative production rates appears large compared to related results from Vega on the column abundances for NH and $NH_2$. Moreels et al. (1986) report column abundance ratios of $NH/OH = 1.4\,10^{-4}$ and $NH_2/OH = 7\,10^{-4}$. Although not directly related to $Q(NH_3)/Q(H_2O)$, these values are quite small compared to our result of $1$–$2\,10^{-2}$. On the other hand, Moreels et al. (1986) report for CH a ratio $CH/OH = 0.05$, and Wyckoff et al. (1986) find from ground-based measurements in the visible spectrum $CH^+/H_2O^+ = 0.04$. Although possibly fortuitous, these results are close to our result, $Q(CH_4)/Q(H_2O) = 0.02$. Drapatz et al. (1986) have attempted a direct measurement of $CH_4$ using high resolution infrared spectroscopic measurements at the $\nu_3$ line of $CH_4$ from the Kuiper Airborne Observatory. Their upper limit of $CH_4/H_2O < 0.04$ is consistent with our measurement from HIS data.

## 7. The radial distribution of ion concentrations

We have derived above the relative production rates $Q(NH_3)/Q(H_2O) = 0.01$–$0.02$ and $Q(CH_4)/Q(H_2O) = 0.02$. We shall refer to this as the "best fit" case and for the purposes of calculations use $Q(NH_3)/Q(H_2O) = 0.015$. In Figs. 8–10, we show model results for the distribution of the light oxygen, nitrogen, and carbon ions inside the contact surface using the rate constants in Table 2 and the value for $Q(H_2O)$ derived from the Giotto NMS data. As seen in Fig. 1a, the $NH_3/H_2O$ abundance ratio drops from a value of 0.01 near 1500 km to a value of 0.005 at 5000 km (due to differential photodissociation of $NH_3$ relative to $H_2O$). As the source of ions is decreasing with increasing distance, the abundance of $NH_n^+$ relative to $H_nO^+$ also decreases with distance as shown in Figs. 8 and 9. In fact the abundance of ammonia drops sufficiently that $H_nO^+$ is not controlled by the $H_3O^+/NH_3$ reaction at larger distances, with the result that $m/q = 19/18$ ap-

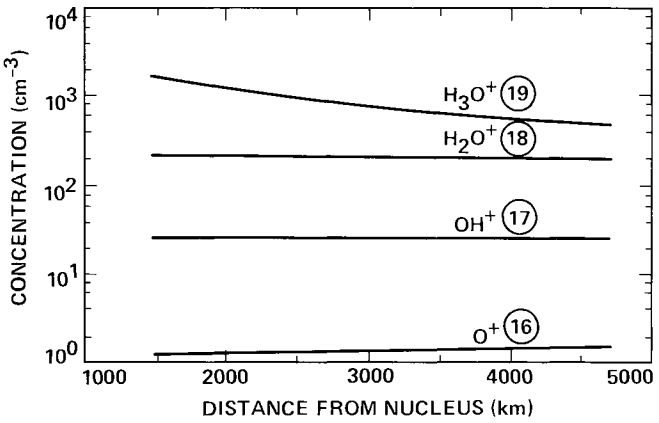


**Fig. 8.** Spatial distribution of the abundances of $H_nO^+$ from the "best fit" case. Masses of ions indicated in circles

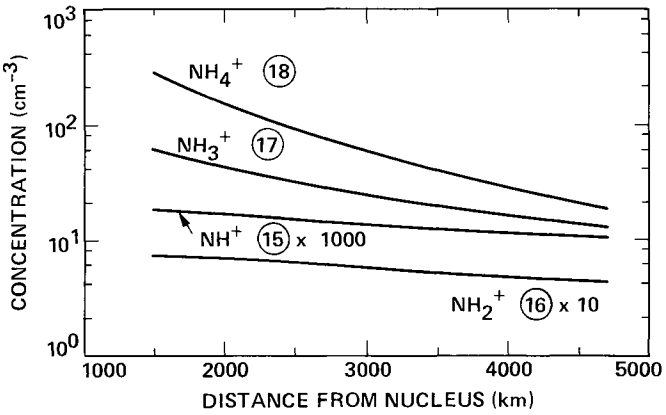


**Fig. 9.** Spatial distribution of the abundances of $NH_n^+$ from the "best fit" case. Masses of ions indicated in circles

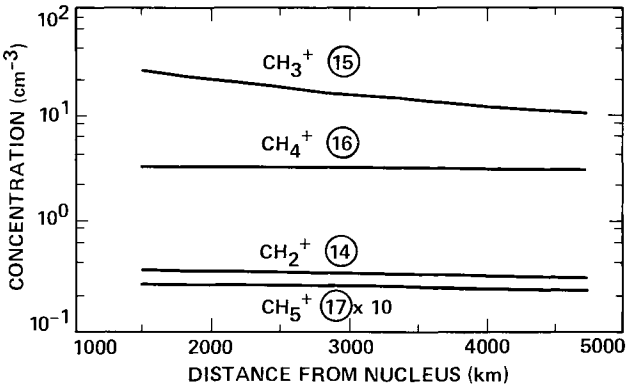


**Fig. 10.** Spatial distribution of the abundances of $CH_n^+$ from the "best fit" case. Masses of ions indicated in circles

proaches the value for the pure water coma (see Fig. 3). At the smallest distances, the contribution to $m/q = 18$ is almost equally from $NH_4^+$ and $H_2O^+$, but it is almost all $H_2O^+$ at the larger distances. While $NH_3^+$ is the main component of $m/q = 17$ within 2500 km, beyond this distance $OH^+$ dominates. At all distances, $CH_3^+$ dominates at $m/q = 15$. These results are of importance in trying to derive isotope ratios from ion mass spectra (see, for example, Eberhardt et al., 1986b).

With the chemistry illustrated in Figs. 2, 4, and 5 in mind, the model results in Figs. 8–10 illustrate two further points. (1) The most abundant hydride ion species are the ones that do not react with $H_2O$. (2) The photolytic source terms for all the ions scale with the spatial profile of the parent species (roughly $r^{-2}$ in the inner coma). The concentrations of those ions destroyed predominantly through reactions with parent species vary very little with distance in the inner coma since the chemical loss factors also have a $r^{-2}$ dependence. However the concentrations of those ions destroyed predominantly by electron recombination decrease with increasing distance from the nucleus more like $r^{-1}$ as would be expected from the analysis of Ip (1986).

## 8. Model uncertainties

The results presented so far have been derived from calculations in which a simple physical model of the inner coma of comet Halley has been assumed: a constant temperature and a variable outflow velocity, which is the same for every species. Our calculations are quite sensitive to the chosen values for the electron temperature $T_e$ as the abundances of the "terminal ions" are controlled by temperature-sensitive electron recombination. The value of $T_e$ we adopted assumed that the ion temperatures measured by Giotto experiments inside the contact surface would be equivalent to the electron temperatures. We have used the temperature measured by the IMS experiment. A somewhat lower value for the ion temperature of 200 K was measured by the NMS experiment (Lämmerzahl et al., 1986). Model calculations using this temperature show a decrease in the ratio $m/q = 19/18$ of 6–20%, the largest change occurring near the contact surface. On the other hand, the results for 15/18 and 17/18 are reduced by $\sim 10\%$ at 1500 km and show minimal differences at the largest distances. These differences would not change our choice of the "best fit" values.

On the other hand, Marconi and Mendis (1984) calculate theoretically an increase in $T_e$ from 4 K to 4000 K within 5000 km from the nucleus. In these computations the electron and ion temperatures are decoupled quite close to the nucleus. We were unable to match the Giotto 19/18 data between 1500 km and 5000 km using the variation in $T_e$ predicted by Marconi and Mendis (1984). High values of $T_e$ yield divergent results at larger distances near the contact surface, and low values give poor agreement at all distances. High values of $T_e$ result in low model values for $m/q = 15/18$ and 17/18, and vice versa. Large variations in $T_e$ with distance will not produce model results that are as constant with distance as is suggested by the Giotto HIS data. Limits on an inferred electron temperature might be derived from our model calculations. Our model results suggest that the electron temperature is approximately a few hundred degrees K and varies by no more than a few hundred degrees K throughout the inner coma.

The model ion chemistry inside the contact surface is close to being in local photochemical equilibrium so that the ion concentrations are relatively insensitive to the adopted velocities for the ions. The velocity profile we have used does affect the distribution of the neutral parent species and, therefore, indirectly the ion profiles. A comparison with the available data discussed earlier in this paper shows that the $H_2O$ distribution is in good agreement with in situ measurements.

Our results are sensitive to uncertainties in several other parameters adopted for these calculations. The accuracy of the

photodissociation and photoionization rates which drive the coma chemistry directly depends on the accuracy of the solar flux and cross-sections utilized. Except at Lyman alpha, the solar flux is not derived from the epoch of the Giotto encounter. Solar variability is possible in the extreme ultraviolet where photoionization occurs. Absorption cross-sections have been measured in the laboratory for various parent molecules, and the branching ratios for the various photoionization channels are becoming more available, but these laboratory data are still incomplete – especially for radicals.

Ion-molecule reactions control the ion densities in the inner coma and our model is very sensitive to this chemistry. Rate constants for these reactions have been measured by a variety of different techniques and good agreement generally exists among the various experimental groups for the reactions relevant to this work (Anicich and Huntress, 1986). Our results are also very sensitive to the values adopted for positive ion-electron recombination coefficients. Values derived from the merged beam experiments (McGowan and Mitchell, 1984) often differ significantly from the results of other techniques. The choice of values used for $H_3O^+$ and $NH_4^+$ recombination coefficients strongly impacts the derived $NH_3$ and $CH_4$ abundances. We have chosen to use the results from microwave experiments since these values result in model $CH_4$ and $NH_3$ abundances which are more consistent with constraints from the HERS experiment.

Calibration of the Giotto HIS data set is not yet completed, and the assignment of data channels to a particular $m/q$ value is not yet completely resolved. Estimates of possible uncertainties are indicated in the figures of the relative $m/q$ ratios.

Taken all together, the cumulative uncertainties in the input parameters and in the Giotto data set can increase the inferred relative production rates derived in this paper by as much as a factor of four, but might decrease the relative production rates by a similar amount. We have not yet pursued an exhaustive error analysis.

## 9. Discussion

The abundance of $CH_4$ and $NH_3$ in the coma are important indicators of the origin of comet Halley. Clues to the origin of comets can be found in the abundances of the elements and in the chemical distribution of each element (J. Geiss, this issue). Comparison of cometary bulk atomic ratios, isotope ratios and chemical composition with these same properties in other solar system and galactic objects may reveal commonalities that suggest possible scenarios for the origin of comets.

The distribution of cometary carbon atoms into CO, $CO_2$, $CH_4$, other hydrocarbons and organic species, and as amorphous solid, graphitic material or trapped radical species, is a critical indicator of the origin of comets. Carbon in the original solar nebula in equilibrium models is mainly in the form of $CH_4$ in the cooler parts of the nebula where the outer planets and comets are believed to have condensed. Lewis and Prinn (1980), however, have shown that this prediction must be modified if the cooling solar nebula gases did not reach thermodynamic equilibrium, and have shown that considerable CO can be retained in the gas phase relative to $CH_4$ under non-equilibrium conditions.

In the interstellar medium, CO is the major form of carbon observed. It is now well established that more that 10% of the whole carbon inventory may be in the form of gas-phase CO in some regions (Black and Willner, 1984). In some cool clouds, atomic carbon can be present in abundance approaching that of CO (Phillips et al., 1980). Knacke et al. (1985) have reported an upper limit to the gas-phase interstellar $CH_4/CO$ abundance ratio of $10^{-2}$. It is generally assumed that any missing elemental carbon is contained in interstellar grains. The detection of the appropriate infrared absorption and/or emission bands has revealed the existence of species in the condensed phase containing CH and/or CO bonds (Leger and Puget, 1984; Lacy et al., 1984; Allamandola et al., 1985). The amount of carbon appears to be less than the amount of gas-phase CO.

The CO abundance in Halley has been reported as 17–20% of water in rocket observations (Woods et al., 1986). The NMS experiment (Eberhardt et al., 1986a) yields a production rate for "native" CO relative to that for $H_2O$ of $\sim 0.07$ with an equivalent production rate for a species easily decomposing to CO. The $CO/H_2O$ value from the Giotto IMS (HERS) experiment is about 0.2 (Balsiger et al., 1986). As reported earlier in this paper, our reanalysis of the NMS data yields a value of 0.042 for $Q(CO_2)/Q(H_2O)$ so that the $CO_2/CO$ ratio is $\sim 0.5$ or less. As pointed out by Prinn (private communication, 1987), the use of coma abundances to infer the composition of the nucleus volatiles implicity assumes that there is no differentiation among these species in the course of being released from the nucleus. Having made that assumption, we note that the rather low ratio of $CH_4$ to CO observed in Halley's coma, $CH_4/CO \sim 0.1$–$0.3$, would tend to argue for an interstellar origin, unless the solar nebula did not reach thermodynamic equilibrium and retained considerable amounts of CO from the pre-nebula cloud phase. On the other hand, the fact that the $CH_4/CO$ ratio in Halley is higher than observed interstellar gas-phase values suggests that Halley may not contain pristine (i.e., totally unprocessed) interstellar material.

Just as for carbon, the distribution of nitrogen into $NH_3$, $N_2$ and various other compounds (such as HCN and organics) provides clues to comet origin and primordial nebula composition. Equilibrium models of the solar nebula yield $NH_3$ as the major form of nitrogen, whereas non-equilibrium models have significant amounts of $N_2$ (Lewis and Prinn, 1980). Models of the chemistry in dense interstellar clouds show $N_2$ and atomic N as the principal forms of nitrogen with smaller amounts of $NH_3$ and HCN (Prasad and Huntress, 1980). The Giotto IMS results show a low abundance for nitrogen in general, and if the present interpretation of the HIS results is correct, then $NH_3$ is the major form of Halley gas phase nitrogen. The upper limit for $N_2$ in Halley's coma is less than 2% of water (from $N_2/CO < 0.1$, Balsiger et al., 1986), so that $N_2/NH_3 < 1$. The ground-based results for HCN show its abundance to be less than 0.1% of water. It is important in any origin hypothesis to explain the low bulk N/O and $N_2/NH_3$ ratios. A potential scenario is that $N_2$ was a major form of nitrogen in the region of cometary origin, but was not retained in cometary condensates due to its volatility. This requires CO to be trapped preferentially relative to $N_2$ in amorphous ice, clathrates, or other solid phases at low temperature.

## 10. Conclusion

We have inferred the production rates for $NH_3$ and $CH_4$ relative to $H_2O$ from the variation with distance of Giotto HIS ion mass

spectra data. The profile for $m/q = 19/18$ is not well simulated by models with a pure water coma. A reasonable fit results for the ratio of production rates $Q(NH_3)/Q(H_2O) = 0.01–0.02$. The presence of a distinct peak at $m/q = 15$, taken together with HERS data at $m/q = 13–15$ at larger distances, indicates the presence of $CH_4$ in the coma gas. The Giotto HIS data for $m/q = 15/18$ is best reproduced with a model production rate ratio $Q(CH_4)/Q(H_2O) = 0.02$. The fit for methane also requires the presence of ammonia in coma gases so that the derived relative production rates are correlated. If a lower value of $NH_3$ is adopted, then less $CH_4$ is needed to fit the $m/q = 15/18$ data.

A number of consequences follow from these results. The partitioning of carbon between $CH_4$ and CO in Comet Halley is unlike speculated conditions in the primitive outer solar nebula or what is seen today in the atmospheres of the giant outer planets. On the other hand, the dissimilarity to interstellar observations suggests that Halley may not be composed of pristine interstellar material. Similarly, the inferred N/O abundance ratio implies a unique origin for Halley.

The work presented in this paper represents the beginning of an analysis procedure that will hopefully reveal the details of the composition of the coma of comet Halley. In this paper we have concentrated on only a limited portion of the Giotto IMS data, and on only $H_2O$, $NH_3$, and $CH_4$. There is a rich harvest yet to be made of the Giotto ion composition measurements.

*Acknowledgements.* This work represents one phase of research carried out at the Jet Propulsion Laboratory, California Institute of Technology, under contract to the National Aeronautics and Space Administration. Partial support also was received from NASA grant NSG-7376 to the California Institute of Technology. The Giotto IMS experiment was supported by the National Aeronautics and Space Administration, the German Bundesministerium für Forschung und Technologie, and the Swiss National Science Foundation.

## References

Allamandola, L.J., Tielens, A.G.G.M., Barker, J.R.: 1985, *Astrophys. J.* **290**, L25

Anicich, V.G., Huntress, W.T.: 1986, *Astrophys. J. Suppl.* **62**, 553

Allen, M., Yung, Y.L., Waters, J.W.: 1981, *J. Geophys. Res.* **86**, 3617

Alge, E., Adams, N.G., Smith, D.: 1983, *J. Phys. B: At. Mol. Phys.* **16**, 1433

Balsiger, H., Altwegg, K., Bühler, F., Geiss, J., Ghielmetti, A.G., Goldstein, B.E., Goldstein, R., Huntress, W.T., Ip, W.-H., Lazarus, A.J., Meier, A., Neugebauer, M., Rettenmund, U., Rosenbauer, H., Schwenn, R., Sharp, R. D., Shelley, E.G., Ungstrup, E., Young, D.T.: 1986, *Nature* **321**, 330

Black, J.H., Willner, S.P.: 1984, *Astrophys. J.* **279**, 673

Despois, D., Crovisier, J., Bockelée-Morvan, D., Schraml, J., Forveille, T., Gérard, E.: 1986, *Astron. Astrophys.* **160**, L11

Drapatz, S., Larson, H.P., Davis, D.S.: 1986, *20th ESLAB Symp* ESA SP-250, Vol. 1, p. 347

Eberhardt, P., Krankowsky, D., Schulte, W., Dolder, U., Lämmerzahl, P., Berthelier, J.J., Woweries, J., Stubbemann, U., Hodges, R.R., Hoffman, J.H., Illiano, J.M.: 1986a, *20th ESLAB Symp* ESA SP-250, Vol. 1, p. 383

Eberhardt, P., Dolder, U., Schulte, W., Krankowsky, D., Lämmerzahl, P., Hoffman, J.H., Hodges, R.R., Berthelier, J.J., Illiano, J.M.: 1986b, *20th ESLAB Symp* ESA SP-250, Vol. 1, p. 539

Haser, L.: 1957, *Bull. Acad. Roy. Belgique (Cl. Sci.)* **18**, 740

Heppner, R.A., Walls, F.L., Armstrong, W.T., Dunn, G.H.: 1976, *Phys. Rev. A.* **13**, 1000

Ip, W.-H.: 1986, *Adv. Space Res.* **5**, 233

Knacke, R.F., Geballe, T.R., Noll, K.S., Tokunaga, A.T.: 1985, *Astrophys. J.* **298** L67

Krankowsky, D., Lämmerzahl, P., Herrwerth, I., Woweries, J., Eberhardt, P., Dolder, U., Herrmann, U., Schulte, W., Berthelier, J.J., Illiano, J.M., Hodges, R.R., Hoffman, J.H.: 1986, *Nature* **321**, 326

Lacy, J.H., Baas, F., Allamandola, L.J., Persson, S.E., McGregor, P.J., Lonsdale, C.J., Geballe, T.R., Van de Bult, C.E.P.: 1984, *Astrophys. J.* **276**, 533

Lämmerzahl, P., Krankowsky, D., Hodges, R.R., Stubbemann, U., Woweries, J., Herrwerth, I., Berthelier, J.J., Illiano, J.M., Eberhardt, P., Dolder, U., Schulter, W., Hoffman, J.-H.: 1986, *20th ESLAB Symp* ESA SP-250, Vol. 1, p. 179

Leger, A., Puget, J.L.: 1984, *Astron. Astrophys.* **137**, L5

Lewis, J.S., Prinn, R.G.: 1980, *Astrophys. J.* **238**, 357.

McGowan, J.W., Mitchell, J.B.A.: 1984, *Electron-Molecule Interactions and their Applications, Vol. 2*, ed. L.G. Christophorou, Academic Press, Orlando, p. 65

McGowan, J.W., Mul, P.M., D'Angelo, V.S., Mitchell, J.B.A., Defrance, P., Froelich, H.R.: 1979, *Phys. Rev. Lett.* **42**, 373; erratum, 1186

Moreels, G., Clairemidi, J., Parisot, J.P., Zucconi, J.M., Festou, M., Bertaux, J.L., Blamont, J.E., Herse, M., Krasnopolsky, V.A., Moroz, V.I., Parshev, V.A., Tkachuk, A. Yu., Gogoshev, M., Gogosheva, Ts., Werner, R., Spasov, S.: 1986, *20th ESLAB Symp* ESA SP-250, Vol. p. 451

Mount, G.H., Rottman, G.J.: 1983, *J. Geophys. Res.* **88**, 5403

Murad, E., Bochsler, P.: 1987, *Nature* **326**, 366

Phillips, T.G., Huggins, P.J., Kuiper, T.B.H., Miller, R.E.: 1980, *Astrophys. J.* **238**, L103

Prasad, S.S., Huntress, W.T.: 1980, *Astrophys. J. Suppl.* **43**, 1

Richtmeyer, R.D.: 1957, *Difference Methods for Initial Value Problems*, Interscience Publ., New York

Rottman, G.J., Barth, C.A., Thomas, R.J., Mount, G.H., Lawrence, G.M., Rusch, D.W., Sanders, R.W., Thomas, G.E., London, J.: 1982, *Geophys. Res. Lett.* **9**, 587

Schloerb, F.P., Kinzel, W.M., Swade, D.A., Irvine, W.M.: 1986, *Astrophys. J.* **310**, L55

Torr, M.R., Torr, D.G.: 1985, *J. Geophys. Res.* **90**, 6675

Winnberg, A., Ekelund, L., Ekelund, A.: 1987, *Astron. Astrophys.* **172**, 335

Woods, T.N., Feldman, P.D., Dymond, K.F.: 1986, *20th ESLAB Symp* ESA SP-250, Vol. 1, p. 431

Wyckoff, S., Wehinger, P.A., Spinrad, H., Belton, M.J.S.: 1986, *20th ESLAB Symp* ESA SP-250, Vol. 1, p. 311